Materials Advances

ROYAL SOCIETY OF CHEMISTRY

PAPER

View Article Online
View Journal | View Issue

Cite this: *Mater. Adv.*, 2025, 6, 2192

Natural-based chalcopyrite nanoparticles as high-performance mineral adsorbents for organic dye removal in water

Sameera Sh. Mohammed Ameen, *[a] Dilsouz D. Hassan,[b] Dlzhar S. Mohammed,[a] Khalid M. Omer, *[c] Dunya A. Latif[d] and Yousif O. Mohammad[d]

Sustainable and natural-based materials with high stability and efficiency for water pollutant removal are vital for advancing sustainable water treatment technologies. This study investigates the use of chalcopyrite mineral nanoparticles (CP NPs), derived from natural and sustainable sources, as efficient, recyclable, and scalable adsorbents for the removal of organic dyes from aqueous solutions. The CP nanoparticles have been thoroughly characterized using spectroscopic and microscopic techniques to determine their size, shape, elemental composition, and the oxidation states of the constituent elements. Due to their high surface area, unique electronic properties, and structural stability, chalcopyrite nanoparticles demonstrate promising potential in capturing and eliminating various dye pollutants from water. The BET analysis of CP NPs reveals a high surface area of 4.5 m^2 g^{-1} with mesoporous structures and varying pore sizes (1.57–112.58 nm). We explored adsorption efficiencies using methylene blue dye, concentrations, and environmental conditions, showing that CP NPs offer high dye removal rates and rapid adsorption kinetics. Under the optimized conditions, a maximum removal efficiency of 99% was achieved using a pH of 8, a contact time of 40 minutes, a dye concentration of 10 mg L^{-1}, and an adsorbent dosage of 0.05 g/100 mL. The experimental data aligned most closely with the Freundlich isotherm model (R^2 = 0.991), suggesting that the adsorption occurred on a non-uniform, multilayered surface. The mechanism of the adsorption was elaborated. This work highlights the natural-based nanoparticles' applicability as cost-effective and sustainable adsorbents for water purification, advancing solutions to manage industrial dye pollutants and improve water quality in environmental systems.

Received 15th January 2025,
Accepted 23rd February 2025

DOI: 10.1039/d5ma00038f

rsc.li/materials-advances

1. Introduction

Adsorption holds significant importance due to its wide-ranging applications in various fields such as environmental remediation, chemical processing, and healthcare.[1–3] In the context of water purification, adsorption plays a crucial role in removing contaminants and pollutants from aqueous solutions, making water safe for consumption and other purposes. Adsorption plays a vital role in water purification by effectively removing a broad spectrum of contaminants, including organic compounds, heavy metals, and pathogens.[4] Adsorption is an easy and effective approach for water treatment because adsorbents, such as activated carbon, have unique surface characteristics that allow them to selectively attract and retain pollutants through physical and chemical interactions. Additionally, adsorption offers advantages such as simplicity, scalability, and cost-effectiveness compared to other techniques like filtration or chemical precipitation, and the use of abundant, renewable adsorbent materials enhances the sustainability of water purification processes.[5]

Using natural-based materials for adsorption offers numerous advantages over synthesized alternatives, including cost-effectiveness, sustainability, scalability, and affordability.[6,7] Natural adsorbents are often more economical due to their abundant and renewable sources, significantly reducing production costs.[8–12] Their scalability allows them to be sourced in large quantities, suitable for various adsorption applications from household filters to municipal treatment plants.[13–16] Furthermore, natural adsorbents are generally safer than synthesized materials, posing fewer risks to both the environment and human health. It is highly important to develop cost-effective, stable, and reliable materials to drive progress in

[a] Department of Chemistry, College of Science, University of Zakho, Zakho, Kurdistan region, 42002, Iraq. E-mail: sameera.m.ameen@uoz.edu.krd
[b] Department of Environmental, College of Science, University of Zakho, Zakho, Kurdistan region, 42002, Iraq
[c] Department of Chemistry, College of Science, University of Sulaimani, Qliasan St. 46002, Sulaymaniyah, Kurdistan region, Iraq. E-mail: khalid.omer@univsul.edu.iq
[d] Department of Geology, College of Science, University of Sulaimani, Qliasan St. 46002, Sulaymaniyah, Kurdistan region, Iraq

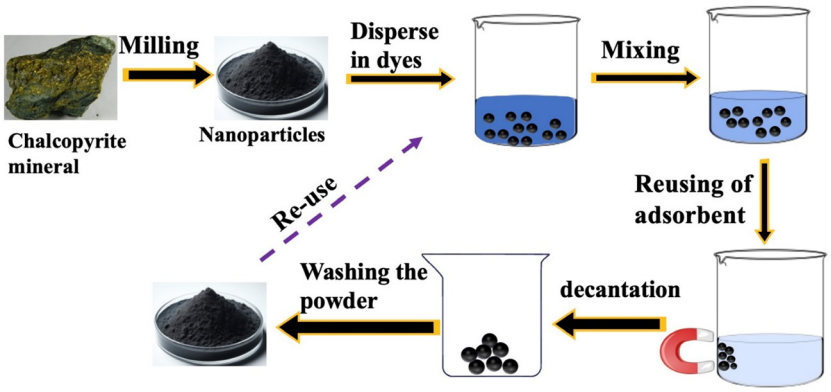

Scheme 1 A scheme showing chalcopyrite nanoparticle preparation and use for removing organic dyes.

critical areas such as adsorption, catalysis,[17–19] and sensing applications.[20–25]

Chalcopyrite, a crucial mineral in both economic and geological contexts, serves as the primary source of copper, comprising copper, iron, and sulfur ($CuFeS_2$). Geologically, chalcopyrite forms in diverse settings including hydrothermal veins, contact metamorphic deposits, and within igneous rocks. Frequently found alongside other sulfide minerals such as pyrite and sphalerite, its distinctive brassy yellow hue and metallic sheen make it easily identifiable. Chalcopyrite remains indispensable in both industrial applications and mineralogical interest.

In this study, we have synthesized a nanoscale powder of chalcopyrite (CP NPs), a mineral that is abundant in the Earth's crust, using a top–down milling approach. The resulting CP NPs will be explored as an adsorbent material for the removal of organic dyes, particularly methylene blue (MB). Chalcopyrite was chosen as an adsorbent because of its remarkable efficiency in removing dye, which makes it highly effective for tackling water contamination issues. Moreover, it is a low-cost, widely available, and abundant mineral, making it a cost-effective choice for large-scale applications. These characteristics, along with its adaptability for functional modifications to improve adsorption capabilities, underscore its potential as an ideal material for dye adsorption. This investigation will focus on understanding the kinetics and thermodynamic properties associated with the adsorption process. Scheme 1 illustrates the preparation process of CP NPs and their potential applications.

2. Experimental section

2.1 Chemicals

All materials and solvents were of analytical grade and used without purification. Sodium hydroxide (NaOH, 99%) and hydrochloric acid 37% were purchased from Roth (Karlsruhe, Germany). Methylene blue (MB) was bought from Sigma-Aldrich (Germany). Ultrapure water was prepared with a Millipore system (18.2 MΩ cm).

2.2 Instrumentation and characterization

Field emission scanning electron microscopy (FESEM) was employed to see the particles and measure the size, shape and morphology of the CP NPs. Energy dispersive spectrum and mapping (EDS) were used for elemental analysis and distribution using MIRA III (TESCAN, Czech). Transmission electron microscopy (TEM) was used to further measure the size and shape of the particles (TEC9G20, FEI, USA) at 200 KV. A powder X-ray diffractometer (PW1730, Netherlands) was used to determine the crystal structure of the CP NPs. Fourier transform infrared spectra (FT-IR) were measured (IRAFFinity-1, Shimadzu). Absorbance spectra were conducted on a Lamda 25 spectrophotometer (PerkinElmer, USA).

2.3 Mineral collection and fabrication of CP nanoparticles

The chalcopyrite mineral was sourced from Bulfat Mountain in the Kurdistan region of Iraq, specifically from a skarn-type chalcopyrite deposit within the Bulfat Igneous Complex geological formation. The rocks from this deposit were extracted using basic equipment and transported to the laboratory for the production of nanosized materials using a milling machine. The synthesis of chalcopyrite nanoparticles (CP NPs) was achieved through a top–down approach, employing a high-energy milling process. Specifically, the pulverization was conducted using a Fritsch Pulverizer 9, a reliable and precise instrument for nanoparticle production. The milling conditions were optimized to ensure uniform particle size and consistent quality, with the machine set to operate for 10 minutes at a speed of 800 revolutions per minute. A stainless steel 1.4125 grinding set was utilized during the process to maintain structural integrity and prevent contamination, resulting in high-purity CP nanoparticles suitable for advanced applications.

2.4 Adsorption experiment

In a typical batch adsorption experiment for MB adsorption, a known amount of adsorbent, CP NPs, is weighed and added to a series of flasks containing varying concentrations of MB solution. The flasks are securely closed and subjected to agitation at a consistent temperature (commonly 298 K) using a shaker set at a specific speed to maintain thorough mixing. At regular intervals, aliquots are taken from the solution, and the concentration of MB is analyzed using a UV-vis spectrophotometer at its characteristic peak absorption wavelength (approximately 664 nm).

The adsorption of MB onto the adsorbent is quantified by comparing the initial and remaining concentrations of MB in the solution. The adsorption capacity at various time intervals is then calculated. This process is typically carried out over a defined duration to determine the equilibrium adsorption capacity (q_e) and to evaluate how parameters such as initial MB concentration, pH levels, temperature, contact time, and adsorbent dosage influence the adsorption behavior.

The maximum adsorption capacity (q_e) can be calculated by using eqn (1) and percentage removal was calculated using eqn (2) as follows;

$$q_e = ((C_i - C_e) \times V)/m \quad (1)$$

$$\% \text{ removal} = ((C_i - C_e))/C_i \times 100 \quad (2)$$

where C_i is the initial concentration (ppm) of MB, C_i is the equilibrium concentration (ppm) of MB, V is the volume (L) of MB solution, m is the mass (kg) of adsorbate.

3. Results and discussion

3.1. Characterization of the NPs

The size, shape, morphology and elemental composition of the nano-sized CP particles were investigated using FESEM, TEM, and EDS analysis, as shown in Fig. 1. The CP particles, as shown in FESEM in Fig. 1A, range from 5 nm to 500 nm.

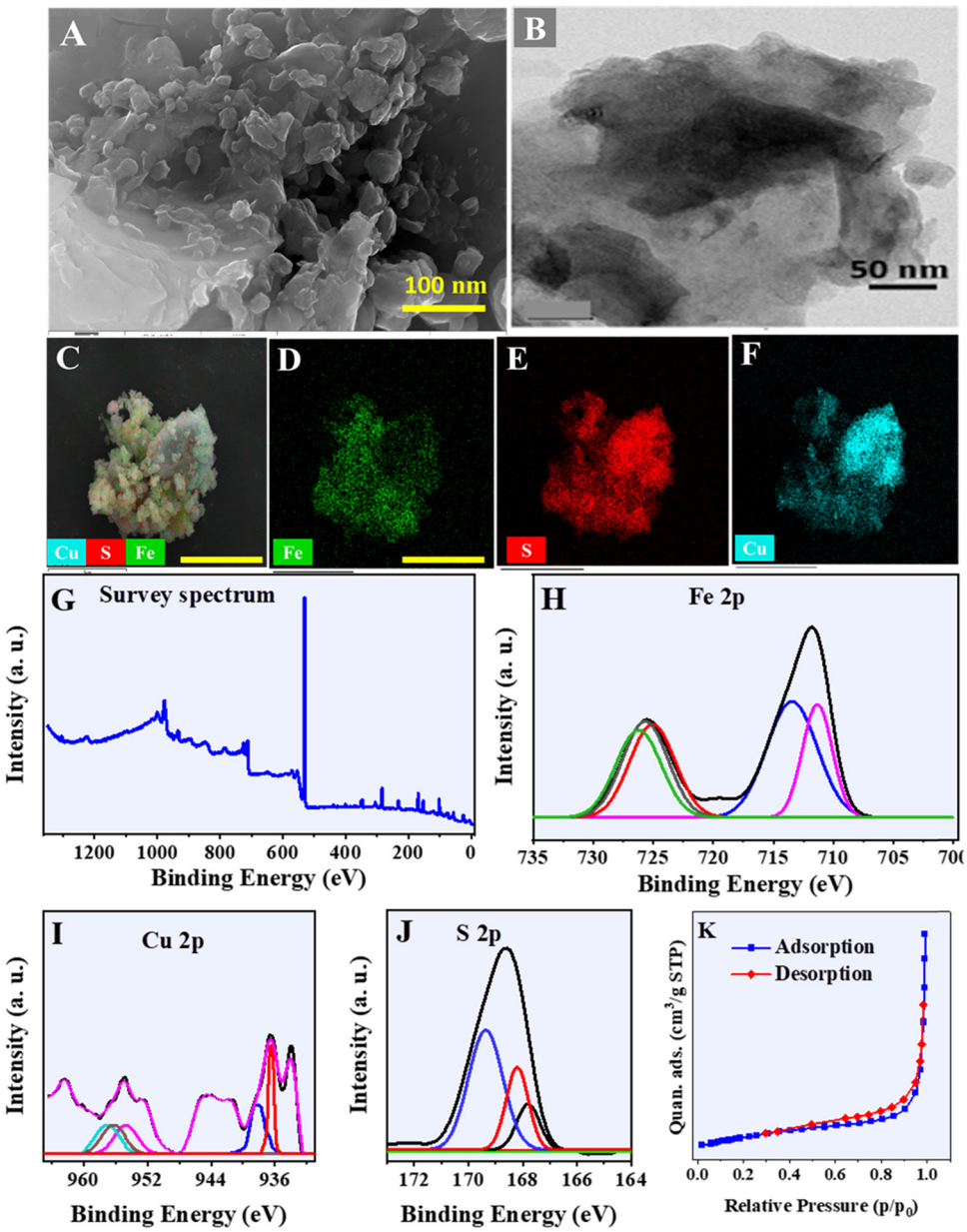

Fig. 1 (A) FE-SEM images of the CP mineralzyme. (B) TEM images of the CP mineralzyme. (C)–(F) EDS mapping of the CP mineralzyme. (G) XPS spectrum survey of the CP mineralzyme. (H) Fe 2p. (I) Cu 2p. (J) S 2p. (K) BET isotherm of the CP mineralzyme.

The TEM image shows clearly the formation of small particles 5 nm, with the presence of aggregated particles as well (Fig. 1B). EDS mapping results (Fig. 1C–F) show the good distribution of the element throughout the particles.

The elemental composition and oxidation states of the CP nanomaterials were further verified using XPS analysis. As shown in Fig. 1G, four peaks could be observed by scanning the XPS spectrum of the CP mineralzyme, which were attributed to S 2p (169.08 eV), Fe $2p_{3/2}$ (712.08 eV), Fe $2p_{1/2}$ (725.1 eV), and Cu $2p_{3/2}$ (933 eV), and Cu $2p_{1/2}$ (954 eV). In the high resolution XPS spectrum of Fe 2p shown in Fig. 1H, the peaks located at 711.2 eV and 724.8 eV are attributed to ferrous (Fe^{2+}), and the peaks at 713.5 and 725.1 eV are attributed to ferric ions (Fe^{3+}).[26] Regarding the resolved spectra of copper peak (Fig. 1I), the peaks at 936.4 and 956.7 eV correspond to Cu^{+} $2p_{3/2}$ and Cu^{+} $2p_{1/2}$, respectively,[27] whereas the peaks at 933.2 and 953.0 eV correspond to Cu^{2+} $2p_{3/2}$ and Cu^{2+} $2p_{1/2}$, respectively.[28,29]

It's important to note that the presence of Cu^{2+} typically leads to the emergence of a satellite peak at approximately 942 eV; usually, these satellite lines belong to cupric oxide Cu(II)O.[30,31] One broad peak around 941–945 eV and centered at 942 eV was seen. The occurrence of the satellite lines of Cu-2p most probably indicates the reactions of Cu^{+} with moisture during exposure to ambient air affecting only the top layers. This is further evidence that Cu^{2+} is present in this structure of chalcopyrite. From here, we can confirm the presence of the two valence forms of copper ions, cuprous and cupric in chalcopyrite. The co-occurrence of different sulfur forms, S^{2-}, S_2^{2-}, and S_n^{2-}, can be observed in the resolved sprat of S, as shown in Fig. 1J, and the peaks at 167.7 eV, 168.2 eV and 169.3 eV are ascribed to S^{2-}, S_2^{2-}, and S_n^{2-}, respectively.[32]

3.2. Nitrogen adsorption desorption isotherm

The Brunauer–Emmett–Teller (BET) technique was used to investigate the porosity, specific surface area, and average pore size and diameter of the CP NPs. The sample specific surface area, volume and average diameter of the pores were analyzed using the BET technique. Depending on the IUPAC category with a hysteresis loop at relative pressure (P/P_0) between 0.3 and 1.0 shown in Fig. 1K, the nitrogen adsorption desorption of CP NPs can be classified as type IV, which indicates the presence of mesopore structures of the prepared CP NPs.

Regarding porosity and surface area, nitrogen adsorption–desorption isotherms were performed (Fig. 1K). The significant adsorption increase at high P/P_0 values suggests the presence of larger mesopores or macropores, enhancing the material's potential for applications in catalysis, adsorption, or gas storage due to their high surface area and accessible pore structure.[33] The calculated total surface area was 4.5 $m^2\ g^{-1}$. The pore size calculation, based on the desorption isotherm data and using Barrett–Joyner–Halenda (BJH) pore size analysis, reveals a range of pore diameters within the material. At higher relative pressures, such as P/P_0 = 0.9831, the pore diameter is approximately 112.58 nm, indicating the presence of larger mesopores. As the relative pressure decreases, smaller pore diameters are observed, reaching around 1.57 nm at P/P_0 = 0.2952. This variation in pore size suggests that the material has a mix of larger and smaller mesopores, potentially influencing its suitability for applications like catalysis or separation, where diverse pore structures may enhance performance.

3.3. Optimizations

Optimization is a highly necessary step in every analytical process as it enhances the sensitivity, and accuracy of the analysis method under various conditions. By refining the parameters, it enables the system to achieve its best performance while accommodating real-world complexities and sample diversity.

3.3.1. Effect of pH. The adsorption capacity of an adsorbent is strongly influenced by the pH value, as it significantly impacts both the surface properties of the adsorbent and the structure of the adsorbate. Fig. 2A and B show the impact of pH on both the capacity and efficiency of MB removal. The adsorption capacity of MB on the CP mineral is optimal between pH 2 and 10 due to the favorable interaction conditions within this range. The surface charge of CP and the ionization state of MB contribute to effective adsorption, with the dye remaining positively charged and the mineral surface conditions supporting this interaction. Additionally, extreme pH levels could lead to solubility or precipitation issues, reducing adsorption. Therefore, the pH range of 2 to 10 provides a stable environment that enhances the adsorption process.[34]

3.3.2. Effect of initial concentration. Regarding the initial concentration, Fig. 2C and D demonstrate the impact of different initial MB concentrations on the adsorption capacity of the CP NPs. It is evident that both adsorption capacity and removal efficiency rise with increasing MB concentration. This occurs because an increased concentration forms a larger concentration gradient between the adsorbate in the solution and the adsorbent surface, promoting the movement of molecules to the adsorbent. As a result, more adsorbate is removed from the solution, and the adsorption capacity may increase.

3.3.3. Effect of contact time. One crucial factor in wastewater treatment for pollutant removal is the determination of the contact time between the adsorbate and adsorbent. Fig. 2E and D illustrate how the adsorption capacity of MB onto CP NPs and the dye removal efficiency vary over time. It was observed that the adsorption capacity and dye removal efficiency increased significantly during the first 10 minutes of contact reaching 1.8 mg g^{-1} and 90%, respectively, and then continued to rise gradually until equilibrium was achieved at 40 minutes. Between 10 and 40 minutes, the increase was only about 10%, which is relatively small. Therefore, the majority of the dye is removed within the first 10 minutes, highlighting the rapid adsorption process of CP NPs.

3.3.4. Effect of temperature. The influence of temperature on the adsorption capacity of CP NPs and the removal of MB was investigated across temperatures ranging from 30 °C to 65 °C (Fig. 2G and H). The temperature study shows that as the temperature increased, both the adsorption capacity and dye removal efficiency also improved. This enhancement is due to the increased mobility of the adsorbent and adsorbate molecules at higher temperatures, which facilitates more frequent interactions between their active sites and thus enhances both adsorption and MB removal efficiency.

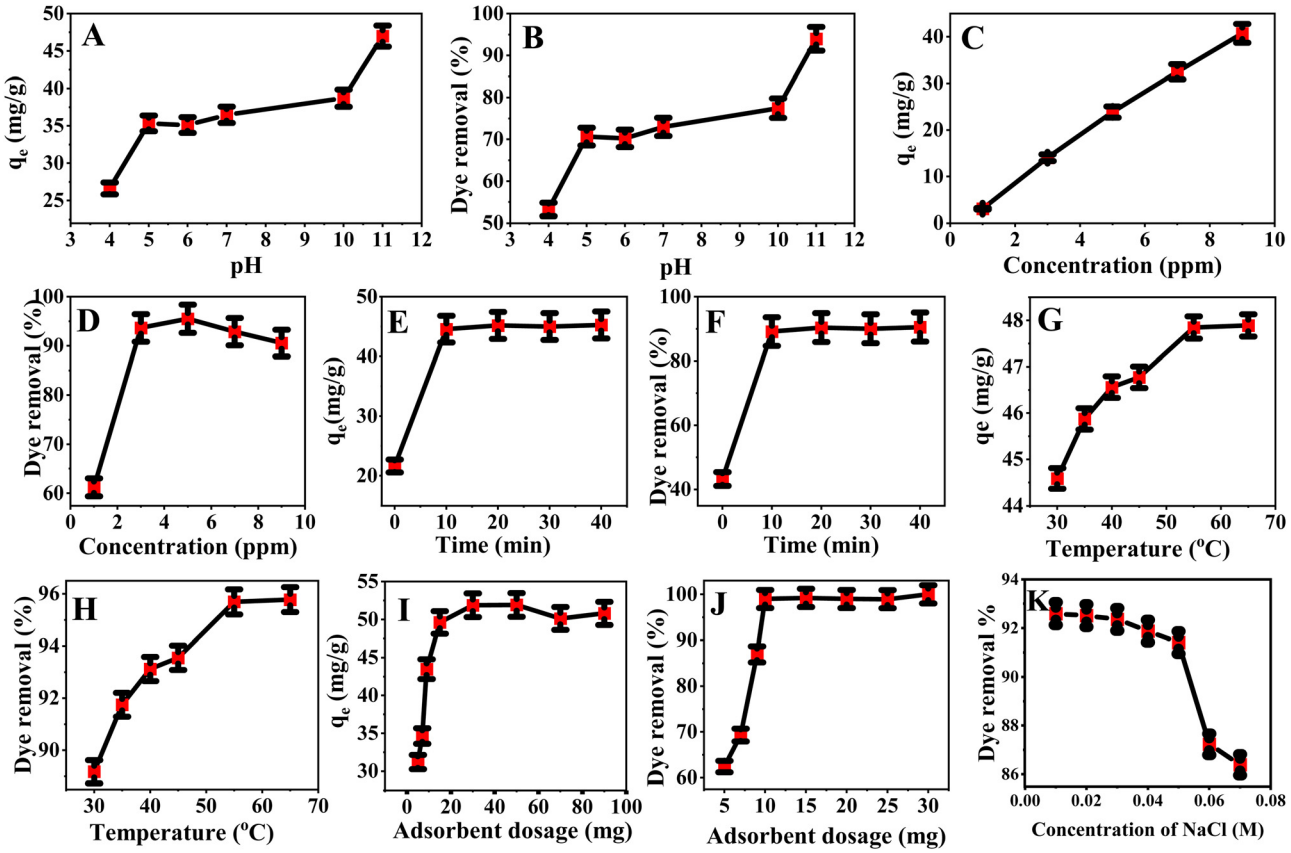

Fig. 2 Effect of five important parameters on the adsorption capacity and dye removal efficiency of MB onto CP NPs. (A) Effect of pH on adsorption capacity. (B) Effect of pH on dye removal efficiency. (C) Effect of concentration on adsorption capacity. (D) Effect of concentration on dye removal efficiency. (E) Effect of contact time on adsorption capacity. (F) Effect of contact time on dye removal efficiency. (G) Effect of temperature on adsorption capacity. (H) Effect of temperature on dye removal efficiency. (I) Effect of adsorbent dosage on adsorption capacity. (J) Effect of dosage on dye removal efficiency. (K) Effect of ionic strength on dye removal efficiency.

3.3.5. Effect of adsorbent dosage. Fig. 2I and J show the effect of CP NP dose on the adsorption capacity of MB onto CP NPs. The adsorption capacity was increased with increasing the adsorbent dose from (5 to 30 mg), this is due to the fact that as the amount of adsorbent increases the number of active sites also increases, which means that there is a higher probability of binding the adsorbate to the active sites of the adsorbent. Moreover, the adsorption capacity starts to stabilize when the adsorbent dosage exceeds 30 mg. This could be due to the fact that at higher dosages, the dye removal efficiency reaches 99%, and the additional adsorbent leads to a surplus of active sites that remain unoccupied. Therefore, the best amount of adsorbent is 0.05 g/100 mL.

3.3.6. Effect of ionic strength. Fig. 2K shows the effect of CP NPs ionic strength on the adsorption capacity of MB onto CP NPs. Various concentrations of NaCl solution were used, reaching up to 0.07 M. The results indicate that the removal efficiency begins to decrease noticeably beyond 0.05 M.

3.4. Adsorption kinetics

To assess the efficiency of adsorption based on the rate of MB uptake onto CP NPs, kinetic studies were conducted. Fig. 3 and the data in Table 1 show that the pseudo-second-order model fits the experimental data well, with an R^2 value of 0.99. In contrast, the pseudo-first-order model has a much lower R^2 value of 0.43. Therefore, the adsorption of MB onto CP NPs follows a pseudo-second-order model, indicating that the process depends on the concentrations of both MB and NPs.

In addition, Elovich and intraparticle diffusion models were investigated in this work. As shown in Fig. 3A, the Elovich model is a kinetic model commonly used to describe the adsorption of chemical species onto solid surfaces, particularly in systems where chemisorption (chemical adsorption) is the dominant mechanism. It is especially useful for heterogeneous adsorption processes, where the adsorption rate decreases over time due to surface saturation or changes in activation energy. The Elovich model parameters, $\alpha = 0.92$, $\beta = 0.35$, provide strong evidence that chemisorption is a key mechanism in the adsorption system. The high initial adsorption rate (α) reflects the adsorbent's efficiency in rapidly capturing the adsorbate, while the moderate desorption constant (β) suggests strong binding and heterogeneous surface interactions.

$$qt = k_{id} \cdot t^{1/2} + C$$

$q(t)$ is the amount of adsorbate (such as a gas or solute) adsorbed at time t; k_{id} = is the intraparticle diffusion rate constant; t = time.

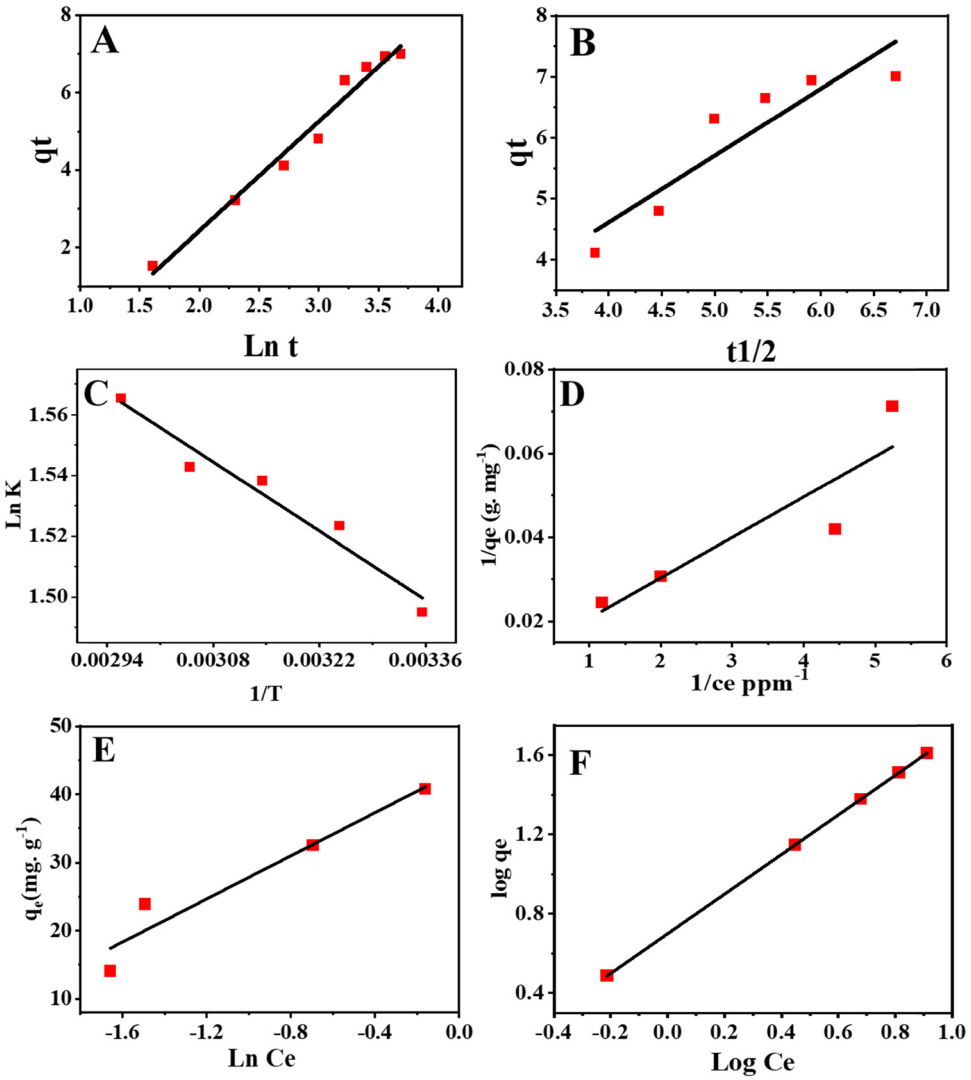

Fig. 3 (A) Elovich model. (B) Particle diffusion. (C) DS Van't Hoff MB. Isotherms of MB onto CP NPs; (D) Langmuir isotherm. (E) Freundlich isotherm. (F) Temkin isotherm.

Table 1 Absorption kinetics, thermodynamics, and isotherm parameters of adsorption of MB onto CP NPs

Kinetic model	Parameter	Value	Thermodynamics						Isotherm models	Parameter	Value
Pseudo first order	q_e (mg g^{-1})	9.480 × 10^{-11}	T (K)	K	ΔG (kJ mol^{-1})	ΔH (kJ mol^{-1})	ΔS (kJ mol^{-1} K^{-1})	R^2	Langmuir	q_{max} (mg g^{-1})	17.94
										K_L	1.16
										R_L	0.08
										R^2	0.71
	k_1 (min^{-1})	1.089	298	4.458	−3.626	1.348	0.017	0.94	Freundlich	$1/n$	1.00
	R^2	0.438	308	4.587	−3.819					K_F	5.00
Pseudo second order	q_e (mg g^{-1})	2616.414	318	4.656	−3.981					R^2	0.99
	k_2 (g mg^{-1} min^{-1})	186 487.100	328	4.677	−4.119				Temkin	B_T	44.30
										K_T (L mg^{-1})	6.94
	R^2	0.99								R^2	0.83
Intra-particle diffusion	K_{id} (mg g^{-1} min$^{-1/2}$)	1.09459									
	C	0.23407									
	R^2	0.8									
Elovich	α	0.9200									
	β	0.35278									
	R^2	0.97									

The results from the particle diffusion model reveal key insights into the rate of particle movement within the system, with a K_{id} of 1.09459 suggesting rapid diffusion. The positive intercept of 0.23407 suggests that the system is not at equilibrium initially, and the R^2 value of 0.8 indicates a strong fit of the model to the observed data. However, the remaining 20% of variation unaccounted for points to the need for further refinement and the inclusion of additional parameters or models to better explain the system's behavior. By addressing these areas, future studies can further improve the accuracy of particle diffusion models and provide more reliable predictions for similar systems.

3.5. Adsorption thermodynamics

To gain a better understanding of how temperature influences adsorption, it is essential to consider the thermodynamic parameters. Parameters such as ΔH, ΔS, and ΔG can be determined using the following equations.[35]

$$\ln K_D = \frac{\Delta S}{R} - \frac{\Delta H}{RT} \quad (3)$$

$$K_D = \frac{q_e}{C_e} \quad (4)$$

$$\Delta G = -RT \ln K_D \quad (5)$$

Fig. 3C displays the van't Hoff plot of $\ln K_D$ *versus* $1/T$. The values of ΔH and ΔS were determined from the plot's slope and intercept. The thermodynamic parameters for the adsorption of MB onto CP NPs are detailed in Table 1. The ΔG values were negative at all temperatures examined and showed a decreasing trend with rising temperature, demonstrating that the adsorption process occurs spontaneously and is thermodynamically more favorable at elevated temperatures. Moreover, the positive enthalpy change (ΔH = +1.348 kJ mol^{-1}) confirms the endothermic nature of the adsorption. The positive entropy change (ΔS = +0.017 kJ mol^{-1} K^{-1}) indicates that the adsorption leads to greater disorder at the interface between CP nanoparticles and MB.

3.6. Adsorption isotherms

Adsorption isotherms are mathematical models used to explain how adsorbate molecules are distributed between the adsorbent and the liquid phase. These models take into account factors such as the uniformity or variability of the adsorbent, the interactions among adsorbate molecules, and the type of coverage on the adsorbent. In this study, the equilibrium data were tested by the Langmuir, Freundlich and Temkin isotherm models.

The Langmuir isotherm suggests that during the adsorption process, a monolayer forms when there is no interaction between adsorbate molecules. The Freundlich isotherm, commonly used for heterogeneous solid catalysts, describes multilayer adsorption through a mathematical relationship. The Temkin isotherm addresses adsorption in heterogeneous systems, assuming that the heat of adsorption decreases linearly with coverage due to interactions between the adsorbent and adsorbate, and that the adsorption binding energies are evenly distributed.[36]

The models are expressed by eqn (6)–(8), respectively

$$\frac{C_e}{q_e} = \frac{C_e}{q_m} + \frac{1}{K_L q_m} \quad (6)$$

$$\ln q_e = \ln K_F + \frac{1}{n} \ln C_e \quad (7)$$

$$q_e = \frac{RT}{b_T} \ln K_T + \frac{RT}{b_T} \ln C_e \quad (8)$$

where q_e is the equilibrium adsorption capacity of MB in (mg g^{-1}), C_e is the equilibrium concentration of MB (ppm), q_m is the monolayer capacity of CP NPs (mg g^{-1}), and K_L represents the adsorption constant in the Langmuir model, while K_F denotes the maximum adsorption capacity constant in the Freundlich model. The parameter n reflects the adsorption intensity in the Freundlich equation. B_T corresponds to the slope expressed in energy units (J mol^{-1}), and K_T signifies the equilibrium binding constant in the Temkin model.

Fig. 3D–F shows the linearized plots and Table 1 shows the results of the applied three isotherm models. According to the values of R^2, the adsorption process fitted more with the Freundlich model of the adsorption isotherm (R^2 = 0.99), which means that the adsorption is of multi-layer type.

Regarding the thermodynamics, the adsorption process is spontaneous, endothermic, and entropy-driven. The negative values of ΔG confirm that the process is spontaneous at all temperatures, with the adsorption becoming more favorable as the temperature increases. The positive ΔH indicates that the process is endothermic, requiring heat input, and the positive ΔS suggests an increase in disorder during adsorption. As temperature rises, the equilibrium constant (K) increases, reinforcing that the process is more favored at higher temperatures, making the adsorption process increasingly efficient and spontaneous with rising temperature. The R^2 value of 0.94 indicates a good fit of the data to the thermodynamic model.

Regarding the isotherm models, the Freundlich isotherm model best fits the experimental data, with a high R^2 = 0.99, indicating a heterogeneous adsorption process with varying affinities across different sites on the adsorbent. The Langmuir model, with a lower R^2 = 0.71, suggests that adsorption does not occur on a homogeneously distributed set of sites, as assumed in Langmuir's theory. The Temkin model, with an R^2 = 0.83, shows a low to moderate fit, indicating some interaction between the adsorbate and adsorbent, but it is less suitable than the Freundlich model. Overall, the Freundlich model is the most appropriate for describing the adsorption behavior in this case.

3.7. Desorption studies

Adsorbent regeneration and reusability following the adsorption process are one of the primary goals of desorption investigations. A key benefit of adsorbents for practical and economical applications is their ability to be reused across multiple adsorption and desorption cycles. In this study, 1.0 M HCl solution was used as an eluent in order to investigate the possibility of reusing CP NPs. Using the batch method, four cycles of consecutive

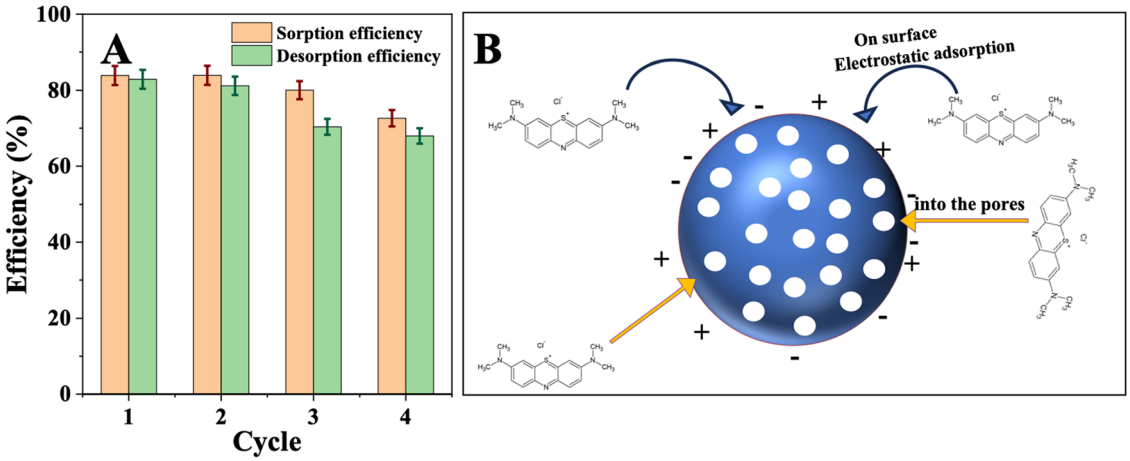

Fig. 4 (A) Sorption/desorption cycles of MB dye onto CP NPs. (B) Scheme of the mechanism of MB with CP NPs.

sorption/desorption tests were carried out. Fig. 4A represents the dye sorption and desorption efficiencies in each cycle. In the first two cycles both the sorption and desorption efficiencies were greater than 80%, and these results suggest that CP NPs show great performance in both processes with minimal loss in their capacity. The decline could be linked to the loss of active sites on the CP NPs, particle aggregation, or blockage of pores due to dye accumulation over successive cycles. Additionally, the nanoparticles may undergo minor structural changes that reduce their overall surface area and adsorption capacity. Despite these declines, the high adsorption and desorption efficiencies across all cycles demonstrate that CP NPs retain good recyclability, though further optimization might be required to maintain their performance over extended usage in real-world applications.

3.8. Adsorption mechanism

The adsorption of MB by CP NPs occurs through two main mechanisms: electrostatic adsorption and pore trapping (Fig. 4B).

1. Electrostatic adsorption: the surface charges of CP NPs attract the oppositely charged MB molecules. The positive charge of MB interacts strongly with the negatively charged functional groups on the CP NP surface, promoting effective adsorption. This process is influenced by factors such as pH and the nanoparticle's surface charge density.

2. Pore trapping: the porous structure of CP NPs allows MB molecules to diffuse into and become trapped within the nanoparticle pores, providing additional active sites for adsorption. The efficiency of this mechanism depends on the alignment of the nanopore size with MB's molecular dimensions.

These dual mechanisms enhance the adsorption capacity of CP NPs, making them effective for environmental remediation, particularly in water treatment.

To sum up and based on reports in the literature, Table 2 shows a comparison between our CP nanoparticles and others. It highlights the satisfactory performance of the CP NPs for dye removal, with an adsorption capacity of 50 mg g^{-1} and 99% efficiency, surpassing several reported adsorbents. For example, silica nanoparticles derived from rice husk achieved only 19.26 mg g^{-1} with >80% dye removal, while biogenic ZrO_2 nanoparticles reached 23.26 mg g^{-1} and 94% efficiency. Though graphene-based nanocomposites showed comparable results, they rely on synthetic and costly processes. The CP NPs in this study provide a sustainable, cost-effective, and scalable alternative, demonstrating their importance in advancing environmentally friendly water treatment solutions.

Table 2 Comparison of adsorption capacity and dye removal efficiency of various adsorbents

Adsorbent	Adsorption capacity (mg g^{-1})	Dye removal (%)	Ref.
SiO_2	19.26	>80	37
ZrO_2	23.26	94	38
Fe_3O_4/chitosan/graphene	47.35	~100	39
Polyaniline/graphene oxide	19.2	99	40
CP nanoparticles	50.00	99	This study

Finally, the economic assessment of the whole process is highly important from an industrial application perspective. The economic assessment of using NPs for pollutant removal highlights their low cost due to chalcopyrite's natural abundance and availability. The preparation costs mainly involve minimal processing, such as grinding and synthesis, which are less expensive than more specialized adsorbents. With an adsorption capacity of 50 mg g^{-1}, the cost per unit of pollutant removal is calculated based on the material's cost and efficiency, resulting in a cost-effective solution. Operational costs, including the energy and disposal of the spent material, are also considered, and the assessment suggests that CP NPs are a competitive, scalable alternative to more expensive adsorbents like activated carbon.

4. Conclusions

Chalcopyrite mineral nanoparticles (CP NPs) were synthesized using a facile top–down milling method and applied for the adsorption of methylene blue (MB) dye from an aqueous solution. Thanks to their relatively high surface area and porosity, CP NPs effectively adsorbed MB, achieving nearly

90% removal within just 10 minutes and 99% removal within 40 minutes, demonstrating exceptionally fast adsorption kinetics that make them highly suitable for industrial-scale applications. The CP NPs exhibit high adsorption efficiency across a wide pH range, with only 0.05 g of adsorbent required per 100 mL of solution for 99% MB removal within 40 minutes. Isotherm, kinetic, and thermodynamic analyses confirm the effectiveness of the process, while recycling studies show that the CP NPs can be reused up to four times without significant loss of performance, highlighting their sustainability and renewability. The natural abundance, low cost, and superior performance of CP NPs as adsorbents ensure their practicality and scalability for large-scale removal of organic pollutants in industrial settings.

Data availability

The authors declare that all the data are available based on the request.

Conflicts of interest

Authors declare that there are no conflicts of interest.

References

1 A. Dąbrowski, Adsorption—from theory to practice, *Adv. Colloid Interface Sci.*, 2001, **93**, 135–224, DOI: 10.1016/S0001-8686(00)00082-8.
2 M. Mozaffari Majd, V. Kordzadeh-Kermani, V. Ghalandari, A. Askari and M. Sillanpää, Adsorption isotherm models: a comprehensive and systematic review (2010–2020), *Sci. Total Environ.*, 2022, **812**, 151334, DOI: 10.1016/j.scitotenv.2021.151334.
3 M. T. Yagub, T. K. Sen, S. Afroze and H. M. Ang, Dye and its removal from aqueous solution by adsorption: a review, *Adv. Colloid Interface Sci.*, 2014, **209**, 172–184, DOI: 10.1016/j.cis.2014.04.002.
4 N. B. Singh, G. Nagpal, S. Agrawal and Rachna, Water purification by using Adsorbents: A Review, *Environ. Technol. Innovation*, 2018, **11**, 187–240, DOI: 10.1016/j.eti.2018.05.006.
5 S. Bolisetty, M. Peydayesh and R. Mezzenga, Sustainable technologies for water purification from heavy metals: review and analysis, *Chem. Soc. Rev.*, 2019, **48**, 463–487, DOI: 10.1039/C8CS00493E.
6 S. Pina, J. M. Oliveira and R. L. Reis, Natural-Based Nanocomposites for Bone Tissue Engineering and Regenerative Medicine: A Review, *Adv. Mater.*, 2015, **27**, 1143–1169, DOI: 10.1002/adma.201403354.
7 A. K. Badawi, R. S. Salama and M. M. M. Mostafa, Natural-based coagulants/flocculants as sustainable market-valued products for industrial wastewater treatment: a review of recent developments, *RSC Adv.*, 2023, **13**, 19335–19355, DOI: 10.1039/D3RA01999C.
8 P. V. Devre and A. H. Gore, Agro-Waste Valorization into Carbonaceous Eco-Hydrogel: A Circular Economy and Zero Waste Tactic for Doxorubicin Removal in Water/Wastewater, *Langmuir*, 2024, **40**, 141–158, DOI: 10.1021/acs.langmuir.3c02256.
9 P. V. Devre, A. S. Patil, D. Sohn and A. H. Gore, Upcycling of spent granular carbon into sustainable and recyclable biopolymeric hybrid hydrogel for highly efficient adsorptive removal of tetracycline pollutant from environmental waters and industrial effluents, *J. Environ. Chem. Eng.*, 2023, **11**, 109368, DOI: 10.1016/j.jece.2023.109368.
10 S. B. Shinde, S. D. Dhengale, O. S. Nille, S. S. Jadhav, A. H. Gore, T. R. Bhosale, N. B. Birajdar, S. S. Kolekar, G. B. Kolekar and P. V. Anbhule, Template free synthesis of mesoporous carbon from fire cracker waste and designing of ZnO-Mesoporous carbon photocatalyst for dye (MO) degradation, *Inorg. Chem. Commun.*, 2023, **147**, 110242, DOI: 10.1016/j.inoche.2022.110242.
11 O. S. Nille, R. S. Patel, B. Y. Borate, S. S. Babar, G. B. Kolekar and A. H. Gore, One-step in situ sustainable synthesis of magnetic carbon nanocomposite from corn comb (MCCC): agricultural biomass valorisation for pollutant abatement in wastewater, *Environ. Sci. Pollut. Res.*, 2023, **30**, 38425–38442, DOI: 10.1007/s11356-022-24847-z.
12 S. S. Mohammed Ameen, F. Algethami and K. M. Omer, Pine needle-derived oxidase-like Mn nanozymes: sustainable nanozyme, scalable synthesis, and visual and colorimetric nitrite detection, *Microchim. Acta*, 2025, **192**, 146, DOI: 10.1007/s00604-025-07024-0.
13 S. Ummartyotin, N. Bunnak and H. Manuspiya, A comprehensive review on modified clay based composite for energy based materials, *Renewable Sustainable Energy Rev.*, 2016, **61**, 466–472, DOI: 10.1016/j.rser.2016.04.022.
14 P. P. Bote, S. R. Vaze, C. S. Patil, S. A. Patil, G. B. Kolekar, M. D. Kurkuri and A. H. Gore, Reutilization of carbon from exhausted water filter cartridges (EWFC) for decontamination of water: an innovative waste management approach, *Environ. Technol. Innovation*, 2021, **24**, 102047, DOI: 10.1016/j.eti.2021.102047.
15 C. S. Patil, A. N. Kadam, D. B. Gunjal, V. M. Naik, S.-W. Lee, G. B. Kolekar and A. H. Gore, Sugarcane molasses derived carbon sheet@sea sand composite for direct removal of methylene blue from textile wastewater: industrial wastewater remediation through sustainable, greener, and scalable methodology, *Sep. Purif. Technol.*, 2020, **247**, 116997, DOI: 10.1016/j.seppur.2020.116997.
16 C. S. Patil, D. B. Gunjal, V. M. Naik, N. S. Harale, S. D. Jagadale, A. N. Kadam, P. S. Patil, G. B. Kolekar and A. H. Gore, Waste tea residue as a low cost adsorbent for removal of hydralazine hydrochloride pharmaceutical pollutant from aqueous media: an environmental remediation, *J. Cleaner Prod.*, 2019, **206**, 407–418, DOI: 10.1016/j.jclepro.2018.09.140.
17 S. S. M. Ameen and K. M. Omer, Temperature-resilient and sustainable Mn-MOF oxidase-like nanozyme (UoZ-4) for total antioxidant capacity sensing in some citrus fruits: breaking the temperature barrier, *Food Chem.*, 2024, **448**, 139170, DOI: 10.1016/j.foodchem.2024.139170.

18 S. S. M. Ameen and K. M. Omer, Multifunctional MOF: cold/hot adapted sustainable oxidase-like MOF nanozyme with ratiometric and color tonality for nitrite ions detection, *Food Chem.*, 2024, **462**, 141027, DOI: 10.1016/j.foodchem.2024.141027.

19 S. S. Mohammed Ameen and K. M. Omer, Pushing Boundaries: Introducing Silver-Based Metal–Organic Framework Oxidase-Like Nanozyme over a Wide-Range Temperature, *ACS Appl. Nano Mater.*, 2024, **7**(17), 20793–20803, DOI: 10.1021/acsanm.4c03725.

20 S. S. Mohammed Ameen and K. M. Omer, Lanthanide and functionalization-free dual-state emitting zinc-based MOFs followed by dual-state detection: ratiometric and color-tonality visual detection of tetracycline in solution and on paper in food and environmental samples, *Microchim. Acta*, 2025, **192**, 22, DOI: 10.1007/s00604-024-06896-y.

21 S. S. M. Ameen and K. M. Omer, Recent Advances of Bimetallic-Metal Organic Frameworks: Preparation, Properties, and Fluorescence-Based Biochemical Sensing Applications, *ACS Appl. Mater. Interfaces*, 2024, **16**, 31895–31921, DOI: 10.1021/acsami.4c06931.

22 S. S. Mohammed Ameen and K. M. Omer, Dual-State Red-Emitting Zinc-Based MOF Accompanied by Dual-Mode and Dual-State Detection: Color Tonality Visual Mode for the Detection of Tetracycline, *ACS Appl. Mater. Interfaces*, 2024, **16**(38), 51376–51383, DOI: 10.1021/acsami.4c13115.

23 S. S. Mohammed Ameen and K. M. Omer, Merging Dual Antenna Effect with Target-Insensitive Behavior in Bimetal Biligand MOFs to Form Efficient Internal Reference Signal: Color Tonality-Ratiometric Designs, *ACS Mater. Lett.*, 2024, **6**, 2339–2349, DOI: 10.1021/acsmaterialslett.4c00845.

24 M. Ameen, S. Sh and K. M. Omer, Three in one: coordination-induced emission for inherent fluorescent Al-MOF synthesis combined with inner filter effect@aggregation-induced emission mechanisms for designing color tonality and ratiometric sensing platforms, *Microchim. Acta*, 2024, **191**, 1–11, DOI: 10.1007/s00604-024-06535-6.

25 S. S. Mohammed Ameen, A. Bedair, M. Hamed, F. R. Mansour and K. M. Omer, Repurposing expired metformin to fluorescent carbon quantum dots for ratiometric and color tonality visual detection of tetracycline with greenness evaluation, *Microchem. J.*, 2024, **207**, 111960, DOI: 10.1016/j.microc.2024.111960.

26 X. Wang, P. Gao, J. Liu, X. Gu and Y. Han, Adsorption performance and mechanism of eco-friendly and efficient depressant galactomannan in flotation separation of chalcopyrite and molybdenite, *J. Mol. Liq.*, 2021, **326**, 115257.

27 A. Ghahremaninezhad, D. G. Dixon and E. Asselin, Electrochemical and XPS analysis of chalcopyrite ($CuFeS_2$) dissolution in sulfuric acid solution, *Electrochim. Acta*, 2013, **87**, 97–112, DOI: 10.1016/j.electacta.2012.07.119.

28 R. G. Acres, S. L. Harmer and D. A. Beattie, Synchrotron XPS, NEXAFS, and ToF-SIMS studies of solution exposed chalcopyrite and heterogeneous chalcopyrite with pyrite, *Miner. Eng.*, 2010, **23**, 928–936, DOI: 10.1016/j.mineng.2010.03.007.

29 P.-Y. Wen, T.-Y. Lai, T. Wu and Y.-W. Lin, Hydrothermal and Co-Precipitated Synthesis of Chalcopyrite for Fenton-like Degradation toward Rhodamine B, *Catalysts*, 2022, **12**(2), 152, DOI: 10.3390/catal12020152.

30 M. Yin, C.-K. Wu, Y. Lou, C. Burda, J. T. Koberstein, Y. Zhu and S. O'Brien, Copper Oxide Nanocrystals, *J. Am. Chem. Soc.*, 2005, **127**, 9506–9511, DOI: 10.1021/ja050006u.

31 M. C. Biesinger, L. W. M. Lau, A. R. Gerson and R. S. C. Smart, Resolving surface chemical states in XPS analysis of first row transition metals, oxides and hydroxides: Sc, Ti, V, Cu and Zn, *Appl. Surf. Sci.*, 2010, **257**, 887–898, DOI: 10.1016/j.apsusc.2010.07.086.

32 L. Jiang, Z. Luo, Y. Li, W. Wang, J. Li, J. Li, Y. Ao, J. He, V. K. Sharma and J. Wang, Morphology- and Phase-Controlled Synthesis of Visible-Light-Activated S-doped TiO_2 with Tunable S4+/S6+ Ratio, *Chem. Eng. J.*, 2020, **402**, 125549, DOI: 10.1016/j.cej.2020.125549.

33 M. Mukoyoshi, H. Kobayashi, K. Kusada, M. Hayashi, T. Yamada, M. Maesato, J. M. Taylor, Y. Kubota, K. Kato, M. Takata, T. Yamamoto, S. Matsumura and H. Kitagawa, Hybrid materials of Ni NP@MOF prepared by a simple synthetic method, *Chem. Commun.*, 2015, **51**, 12463–12466, DOI: 10.1039/C5CC04663G.

34 X. Wang, T. Li and C. Ma, A novel ICT-based chemosensor for F- and its application in real samples and bioimaging, *J. Hazard. Mater.*, 2021, **413**, 125384, DOI: 10.1016/j.jhazmat.2021.125384.

35 K. R. Ahmed, D. S. Mohammed and F. M. Ali, Synthesis Of A New Adsorbent Based On The Mild Dealuminated Binder Free Granular Y Zeolite, *Sci. J. Univ. Zakho.*, 2023, **11**, 333–345.

36 A. M. M. Vargas, A. L. Cazetta, M. H. Kunita, T. L. Silva and V. C. Almeida, Adsorption of methylene blue on activated carbon produced from flamboyant pods (Delonix regia): study of adsorption isotherms and kinetic models, *Chem. Eng. J.*, 2011, **168**, 722–730, DOI: 10.1016/j.cej.2011.01.067.

37 L. Usgodaarachchi, C. Thambiliyagodage, R. Wijesekera and M. G. Bakker, Synthesis of mesoporous silica nanoparticles derived from rice husk and surface-controlled amine functionalization for efficient adsorption of methylene blue from aqueous solution, *Curr. Res. Green Sustainable Chem.*, 2021, **4**, 100116.

38 A. Alagarsamy, S. Chandrasekaran and A. Manikandan, Green synthesis and characterization studies of biogenic zirconium oxide (ZrO_2) nanoparticles for adsorptive removal of methylene blue dye, *J. Mol. Struct.*, 2022, **1247**, 131275.

39 H. V. Tran, L. T. Hoang and C. D. Huynh, An investigation on kinetic and thermodynamic parameters of methylene blue adsorption onto graphene-based nanocomposite, *Chem. Phys.*, 2020, **535**, 110793.

40 E. A. El-Sharkaway, R. M. Kamel, I. M. El-Sherbiny and S. S. Gharib, Removal of methylene blue from aqueous solutions using polyaniline/graphene oxide or polyaniline/reduced graphene oxide composites, *Environ. Technol.*, 2020, **41**(22), 2854–2862, DOI: 10.1080/09593330.2019.1585481.